Computational and Theoretical Chemistry 1241 (2024) 114877

Contents lists available at ScienceDirect

Computational and Theoretical Chemistry

journal homepage: www.elsevier.com/locate/comptc

Comparative study of CO adsorption on Au, Cu, MoO_2 and MoS_2 2D Nanoparticles

N. Ngom [a], A.J. Etindele [b], N.F. Andriambelaza [c], C. Nithaya [d], A.S. Wakata [e], S. Kenmoe [f,*]

[a] University of Yaounde I, Department of Physics, Yaounde, Cameroon
[b] Higher Teachers Training College, University of Yaounde I, Yaounde, Cameroon
[c] Department of Physics, University of Pretoria, Pretoria, 0002, South Africa
[d] University of the Witwatersrand, Faculty of Science, Johannesburg, South Africa
[e] Materials Science Laboratory, Department of Physics, Faculty of Science, University of Yaounde I, Cameroon
[f] Department of Theoretical Chemistry, University of Duisburg–Essen, Universitätsstr. 2, 45141 Essen, Germany

ARTICLE INFO

Keywords:
2D nanoparticles
Density functional theory (DFT)
CO
Adsorption
Reactivity descriptors
Charge transfer
Au
Cu
MoO_2
MoS_2
Morphology
Size

ABSTRACT

This study focuses on a comparative analysis of the electronic properties of triangular, irregular hexagonal, and octagonal 2D nanoparticles containing 10, 12, and 14 motifs, made of Au, Cu, MoO_2, and MoS_2. The investigation was carried out using density functional theory. The formation energies and vibrational frequencies demonstrate that the 2D nanostructure configurations can exist as stable structures. Edge atoms with lower coordination numbers than central atoms, are the preferred sites for CO adsorption. Using orbital-weighting dual descriptors calculated from Fukui functions enabled the identification of a majority nucleophilic attack sites in Au and Cu nanoparticles, while MoO_2 and MoS_2-based nanoparticles present almost as many electrophilic sites as nucleophilic sites. The charge transferred between the nanostructures and the CO molecule and the redistribution of the projected density of states were used to assess the strength of interfacial bonds and the nature of the fundamental interaction involved in the bonding.

1. Introduction

Human industrial as well as domestic activities release dangerous pollutants and contaminants that contribute to the environment degradation [1]. Among these harmful pollutants is carbon monoxide (CO), which mainly comes from emissions resulting from the incomplete combustion of fossil fuels. This highly toxic substance can lead to health damages. These include headaches, gastrointestinal disorders, dizziness, weakness, seizures, coma and death by asphyxiation [2]. One of the main channels through which carbon monoxide could be eliminated is its oxidation to form carbon dioxide. This reaction is unfavored at room temperature due to its high activation barrier. Heterogeneous catalysis offers the possibility to speed-up and achieve CO oxidation. Silver based catalysts [3], copper [4], metal oxides [5,6] or noble metals [7,8] have been used for this purpose. Metal based catalysts, particularly, copper and gold exhibit high catalytic activity, selectivity, thermal stability and ease of recovery [4,7]. Recently several theoretical and computational studies have provided deep atomistic insight into the complex interplay between the factors governing the catalytic performance of gold and copper bulk surfaces and nanoclusters of various dimensions [9–12].

Although metals exhibit exceptional yields for the catalytic oxidation of CO, their scarcity and high cost represent a major obstacle to their large-scale use. In addition, they could be quickly deactivated under certain temperature and pressure.[13] This has triggered the interest for alternatives. In recent years, theoretical and experimental research has been carried out on transition metal dichalcogenides (TMDCs) as they are seen as an alternative for low-cost oxidation of carbon monoxide [14–16]. This stems from their unique electronic structure, the multiple oxidation states of the transition metals, their large active surface due to their two-dimensional sheet-like arrangement, and their stability [17–19]. Compared to bulk catalysts, nanostructured catalysts of lower dimensions present beneficial properties for oxidation. These include their high specific surface area [20], the presence of multiple active sites [21], size and shape induced physical and chemical properties [22], good stability [23], doping and functionalization [24,25]. The adsorption of CO on metals and TMDCs and its subsequent oxidation has been the subject of intense investigation.

* Corresponding author.
E-mail address: stephane.kenmoe@uni-due.de (S. Kenmoe).

https://doi.org/10.1016/j.comptc.2024.114877
Received 13 May 2024; Received in revised form 30 August 2024; Accepted 14 September 2024
Available online 18 September 2024

Increasingly efficient computational techniques have been used to accurately describe the binding sites and energies with respect to the elemental composition of surfaces [26,27]. The d-band center has been used to predict the reactivity of metals such as gold [28] and even TMDCs like MoS_2 sheets [29]. Mpourmpakis et al. used the coordination number and curvature angle to unravel how the size, shape, and symmetry of metal nanoparticles affect their electronic properties and, consequently, their interaction with CO [30]. Unlike metals, TMDCs have a layered structure with covalently bonded metal and chalcogen atoms. Their electronic structure is dominated by the hybridization of metal d-orbitals and chalcogen p-orbitals. To describe the reactivity of TMDCs and compare it to that of metal surfaces, descriptors that would better capture their unique electronic structure of the former are necessary to improve the level of understanding of structure-to-activity relationship to that of the latter.

Despite the efforts for the search of alternatives to metal catalysts, one of the main challenges that remain when considering 2D nanoparticles as potential candidates is the availability of descriptors that predict both the most favorable reactive sites and the type of on-site interaction with the toxic molecules, as a function of the composition, size and shape of the nanoparticles. The level of complexity both in the nature of the active sites and in the interaction of the adsorbates with metal chalcogenide surfaces renders the way towards a universal character of descriptors more tricky, and thus, calls for more comprehensive studies. One of the prior steps towards an efficient and rational design of the catalytic nanoparticles is the determination of the sensing properties. An accurate determination, both qualitatively and quantitatively, of the charge transfer between catalyst surface and the adsorbate is crucial to achieve selective detection of the toxic molecules. Moreover, to enable non destructive desorption and consequently efficient catalyst recovery, a comprehensive understanding of the adsorption and the underlying catalyst relaxation trends is necessary [31,32].

In this paper, we explore the possibilities of sensors to toxic gas such as CO molecules based MoO_2 and MoS_2 nanoparticles and compare their properties with Au and Cu nanoparticles of the same shapes. We investigate the structure and stability of 2D nanoparticles with different topologies including motifs of 10, 12 and 14 Au, Cu, MoO_2 and MoS_2. We compute and analyze the electronic structure and reactivity descriptors of the different nanoparticles. We further monitor the adsorption of CO on the potential active sites and combine charge transfer and density of states analyses to address the nucleophilic or electrophilic character of the interaction between the nanoparticles and the CO molecule.

2. Computational details

The total energies of the materials systems were calculated using density functional theory (DFT) as implemented in the Quantum Espresso [33] and Gaussian [34] packages. Quantum Espresso was used to optimize the different clusters, to determine the coordination number (CN), and finally calculate the charge density difference between the cluster and carbon monoxide (CO). Gaussian was used to calculate the infrared frequencies in order to extract the vibrational frequencies. No symmetry restrictions or/and geometry constraints were applied during optimization of the clusters using both packages. Conceptual density functional theory (CDFT) was used to predict the chemical reactivity [35] and we utilized the Multiwfn code developed by Lu et al. [36] to plot color contour maps of the electron density. VESTA [37] was also used to plot the charge density on the different systems.

For all calculations, Perdew–Burke–Ernzerhof (PBE) formulation of the generalized gradient approximation (GGA) was used [38] to account for the exchange and correlation effects. The dispersion interactions were taken into account using the Grimme D3 correction [39]. Marzari–Vanderbilt cold smearing [40] with a width of 0.005 Ry was used to converge the systems optimization. The calculations on the clusters were performed using a 1×1 unit cell with a distance of 20 Å. A plane wave basis with a cutoff energy of 60 Ry for wavefunctions and 240 Ry for the charge densities was used to expand the wave functions. Furthermore for Gaussian calculations, the PBE0 functional [41] and LANL2DZ basis set were used within Gaussian 16 for accurate description of the transition metals orbitals [42]. The compatibility of the results obtained with the packages was tested by comparing key structural parameters of the nanoclusters. As it can be seen from Table S1 in the Supporting Information, they agree reasonably.

The energetically favorable nanostructures were investigated by calculating the formation energies defined as follows:

$$E_{f_1} = \frac{E(total)}{N} - E_x, \qquad E_{f_2} = \frac{E(total)}{N} - E_y - E_z \tag{1}$$

where E_{f_1} corresponds to the formation energies of Au, Cu while E_{f_2} is the formation energies of MoO_2 and MoS_2. E(total) is the total energy of the nanostructure, E_x is the energy of Au/Cu, E_y is the energy of Mo, E_z is the energy of O_2/S_2 and N the number of Au/Cu atoms or units of MoO_2/MoS_2 in the compound.

The adsorption energy (E) of CO on the surfaces was calculated using the following formula:

$$E = E_{surface+gas} - E_{surface} - E_{gas}, \tag{2}$$

where $E_{surface+gas}$, $E_{surface}$, E_{gas} are the total energy of the nanocatalyst together with the gas molecules, the energy of the isolated nanocatalyst, and the energy of the isolated gas molecule, respectively.

3. Results and discussion

3.1. Structure and stability

MoO_2 and MoS_2 can crystallize on graphene layers as 2D ultrafine nanoparticles [43,44]. MoO_2 and MoS_2 in their 2H phase belong to the P63/mmc space group. In contrast, gold and copper generally prefer a bulk structure and crystallize into face-centered cubic systems. However for this work, we have constructed 2D gold and copper nanosheets of different shapes and sizes, this with the aim of obtaining 2D nanoparticles of the same shape as that of TMDCs. Fig. 1 displays the optimized structures of 2D nanoparticles based on Au, Cu, MoO_2, and MoS_2, obtained from DFT calculations. Three geometrical shapes were considered due to their high stability (low formation energy) for given numbers of basic motifs: the triangular, the irregular hexagonal and the octagonal shapes. The basic motif being a gold atom, a copper atom, a MoO_2 molecule or a MoS_2 molecule. The triangular shape includes 10 basic motifs, the irregular hexagonal shape 12 basic motifs and the octagonal shape 14 basic motifs.

The formation energies per unit motifs of the different structures are listed in Table 1. It is interesting to note that all the energies are negative. This suggests that the formation of these structures is energetically favorable. Moreover, the geometrical shapes of MoO_2 and MoS_2 are more stable than those of Au and Cu for the same number of basic motifs. While the formation energies of the metallic nanostructures are found into the range of −2.16 to −2.57 eV, those of the transition metal chalcogenides can be up to an order of magnitude lower, ranging from −12.99 to −15.83 eV. It can be generally observed that the stability increases with the size of the nanostructure. On Au and Cu nanostructures, there is an energy gain 170 meV and 200 meV, respectively, when the size of increases from 10 to 12 motifs. Less energy is gained when the metallic nanostructures are enlarged to 14 motifs (20 meV and 50 meV for Au and Cu, respectively). Similar trends are observed for MoO_2 and MoS_2. The stabilization energies read 250 meV and 170 meV from 10 to 12 motifs nanostructures and 10 meV and 110 meV from 12 to 14 motifs. The larger stabilization energy of the MoO_2 and MoS_2based geometrical shapes can be explained by the fact that they tend to agglomerate preferentially in sheet-like structures

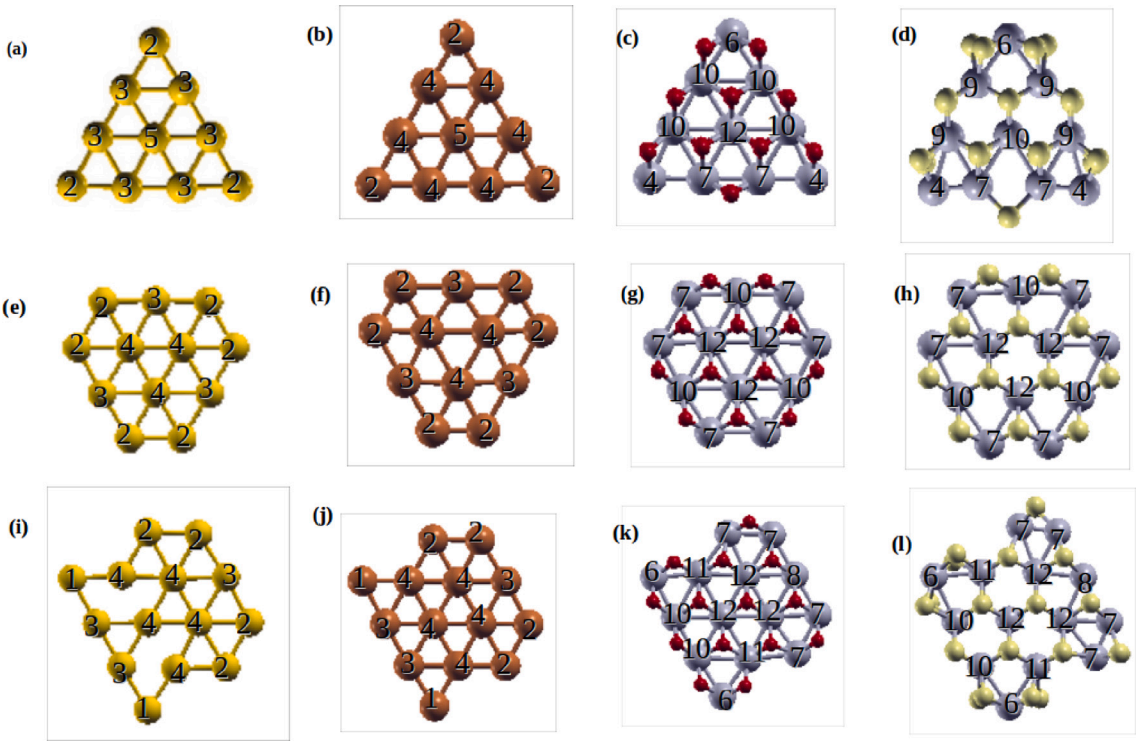

Fig. 1. First, second and third rows represent the optimized nanostructures for Au, Cu, MoO_2, MoS_2; in (a–d) triangular, (e–h) irregular hexagonal, (i – l) octagonal shapes. These shapes correspond to a number of atom x = 10, 12 and 14, respectively. The coordination number of each probable site of fixation are indicated in each figure. With atom colors: Au (gold), Cu (brown), Mo (gray), O (red) and S (yellow).

rather than in bulk. The formation energies of bulk MoO_2 and MoS_2 are found within the range: −2.64 to −3.12 eV per MoO_2 unit [45] and −2.28 to −2.96 eV per MoS_2 unit [46], respectively.

It can also be seen from Table 1 that in the metallic nanostructures displayed in Fig. 1-a,b,e,f,i and j, the bond lengths are very similar, independently of the size of the nanostructure. This may explain the low energy gain observed upon the formation of larger nanostructures as few relaxations are needed. However, in MoO_2 and MoS_2 nanostructures, one can observe a considerable change in bond length distances both for metal–metal (Mo-Mo) and metal-chalcogen (Mo–O or Mo–S) bonds. In the case of MoO_2 (Fig. 1-c, g and k), while the former shows a magnitude of elongation of 0.1 to 0.3 Å, a drastic contraction of the Mo–O bond (0.7 Å) is observed when the nanostructure size increases from 10 to 12 motifs. This is in line with the 250 meV energy gain reported above. The Mo-O bond length remains almost unchanged when the size is enlarged to 14 motifs. As a consequence, the formation energy is not altered. This shows the role of the metal–oxygen bond in the stabilization of the nanostructures. At the critical value of 1.88 Å, it costs the same energy to stabilize the 12 and 14 motifs nanostructures. In MoS_2 nanostructures (Fig. 1-d, h and l), the magnitude of relaxations are similar, but the driving force is reversed. In fact, the metal-chalcogen bond length is barely affected by the size increment (0.15 Å, at most) while the metal–metal bond is elongated by about 0.7 Å. In general, the metal–sulfur bond, longer than the metal–oxygen bond in MoO_2, undergoes oscillatory relaxations of very small amplitude. This stems more likely from the larger size of the S atom and the exclusion volume around it. This trend is in line with the finding reported in Ref. [29] where the authors claimed that the metal d-band center could be used as a single electronic descriptor for the structure and adsorption on MoS_2 nanosheets.

We further investigated the mechanical stability of the nanostructures by calculating their vibrational frequencies. Table 2 presents the first three vibrational frequencies of the different nanostructures reported in Fig. 1. The fact that all vibration frequencies are positive

Table 1
Topologies (number of motif units), formation energy (E_f) per motif unit and interatomic distances of Au, Cu, MoO_2 and MoS_2 nanostructures.

Nanostructure	Topology	E_f(eV)/motif	distance (Å)
Au	10	−2.16	2.72 – 2.63
	12	−2.33	2.69 – 2.71
	14	−2.35	2.60 – 2.69
Cu	10	−2.32	2.38 – 2.39
	12	−2.52	2.37 – 2.38
	14	−2.57	2.38 – 2.30
MoO_2	10	−15.57	Mo-Mo: 2.58 – 2.76 Mo-O: 2.55 – 2.79
	12	−15.82	Mo-Mo: 2.90 – 2.79 Mo-O: 1.88 – 2.05
	14	−15.83	Mo-Mo: 2.67 – 2.60 Mo-O: 1.88 – 2.03
MoS_2	10	−12.99	Mo-Mo: 2.29 – 3.04 Mo-S: 2.23 – 2.53
	12	−13.16	Mo-Mo 3.02 – 2.97 Mo-S: 2.36 – 2.39
	14	−13.27	Mo-Mo: 2.94 – 2.87 Mo-S: 2.33 – 2.44

indicates that the nanostructures remain stable under a small external perturbation. This finding is in agreement with the observations reported in the experimental work performed by J.V. Lauritsen and *al.* [47] and in which triangular MoS_2 shapes were observed using atom-resolved Scanning Transmission Microscopy. The saturation of the nanoparticles edges by chalcogens was found to be the driven force for the stabilization of the nanostructures. The same holds in our computed triangular transition metal dichalcogenide nanostructures. Edges in triangular MoS_2 and MoO_2 are both populated by chalcogens in the outermost layers. Besides, as empirically deduced in the same study, the number of motifs unit equal to 10 corroborates well the even magic numbers that can form a triangular nanostructure. Nevertheless,

Table 2
The three first vibrational frequencies of the different nanostructures, wavenumber ($\bar{\nu}$).

Nanostructure	$\bar{\nu}$ (cm^{-1})	Nanostructure	$\bar{\nu}$ (cm^{-1})
	4.03		23.28
Au(10)	16.34	MoO_2(10)	25.10
	18.20		63.65
	17.94		41.21
Au(12)	42.67	MoO_2(12)	46.78
	42.68		56.65
	8.22		56.89
Au(14)	21.13	MoO_2(14)	57.86
	25.87		77.93
	72.40		11.48
Cu(10)	84.48	MoS_2(10)	32.87
	100.65		52.77
	22.46		16.35
Cu(12)	30.41	MoS_2(12)	44.05
	87.92		69.58
	15.60		31.62
Cu(14)	47.60	MoS_2(14)	42.58
	47.74		44.72

although these authors reported that only triangular shapes could be observed, the values of the formation energies and vibrational frequencies found in the present work suggest that the irregular hexagonal as well as the octagonal shapes could also be observed. Yet, one would need to investigate the thermodynamic stability of these nanostructure under O- and S-rich conditions, respectively. Information about two-dimensional (2D) nanostructures of Au and Cu is scarce. Nevertheless, our computed formation energies and vibrational frequencies also suggest that they could exist or be synthesized. However, these nanostructures would be metastable compared to their 3D counterparts which have lower formation energies ranging from −3.1 to −3.7 eV per atom [48–50].

3.2. Reactivity descriptors

The nanostructures reactivity and particularly their ability to exchange charges with adsorbates plays a determining role in their catalytic performance. Reactivity descriptors such as coordination number [51], orbital-weighted Fukui functions, and orbital-weighted dual descriptors [52] are valuable tools for evaluating the catalytic behavior of nanostructures. We have investigated these descriptors for the different nanostructures under consideration in this work.

3.2.1. Coordination numbers (CN)

We started by addressing the coordinative environment of the two groups of nanoparticles, Au and Cu on one hand, and MoO_2 and MoS_2 on the other hand. Fig. 1 schematically shows the structural motifs with the coordination numbers assigned to each of their atoms. The coordination number is taken to be number of bonds formed between a central metal atom or ion and the surrounding atoms or groups of atoms, known as ligands. The coordination number of MoO_2 and MoS_2 is higher than that of Au and Cu. This can be explained by the fact that while gold (Au) and copper (Cu) are surrounded by monoatomic neighbors, molybdenum (Mo) in MoO_2 and MoS_2 nanoparticles are surrounded by other Mo atoms, oxygen (O) or sulfur (S) ligands, respectively. This allows each molybdenum atom to bond with a larger number of neighboring atoms, resulting in a higher coordination number. In general, it can be seen that the edge atoms have lower CNs than the central atoms in all the structures. This under-coordination reflects the presence of incomplete molecular orbitals, which are likely to facilitate the adsorption making the edge atoms potential active sites for molecule adsorption.

3.2.2. Orbital-weighted dual descriptors

In numerous studies, edges atoms have been found to play a crucial role in devices design and application. This has triggered stimulating studies on their determination and characterization in order to optimize the properties or functionalization [53,54]. For deeper insight into the interaction of these sites with adsorbates, we have investigated the local reactivity and electronic properties of the nanostructures. We used orbital-weighted dual descriptors to identify the electrophilic and nucleophilic sites. The results obtained are presented in Fig. 2. This figure shows the isosurfaces of the orbital-weighted dual descriptors obtained for each system. The sites favorable to electrophilic attacks are represented in green, while those favorable to nucleophilic attacks are shown in blue.

Regardless of the (metallic) nanostructure (Fig. 1-a, b, e, f, i and j), it can be observed that the edge atoms in Au and Cu nanostructures exhibit higher charge densities compared to the atoms located in the center, making the former more susceptible to nucleophilic attacks. However, it is interesting to note that considering the iso-densities, a nucleophilic attack could occur at the central sites. This is the case, for example, for Cu (Fig. 2-f). Meanwhile, on certain atoms located at the edge of the Au (Fig. 2-a) and Cu (Fig. 2-b) nanoparticules, electrophilic attacks could also occur. Thus, Au and Cu are more predisposed to nucleophilic attacks but could also participate in electrophilic reactions under certain conditions. On the other hand, for the MoO_2 and MoS_2-based nanostructures, the dual descriptors reveal the presence of sites that are both electrophilic and nucleophilic, with higher charge densities on the edge atoms (Fig. 2-c, d, g, h, k and l). This indicates that these nanostructures can undergo both nucleophilic and electrophilic attacks, making them potentially more versatile in terms of catalytic reactivity. One should note, however, that for MoS_2 nanostructures, the nucleophilic sites are mainly located on the sulfur atoms.

3.3. CO adsorption and electronic structure

To study the adsorption of CO on the nanostructures, several potential adsorption sites were considered, including central and edges sites, as well as different CO molecule orientation with respect to the surface plane. Motivated by the stronger reactivity observed at the under-coordinated edges sites, the adsorption of CO was investigated at the nanostructures edges considering both nucleophilic and electrophilic sites. The optimized structures, their corresponding adsorption energies and charges transferred from the nanoparticle to the molecule or vice versa at the main active sites are displayed in Fig. 3 and Fig. 4, respectively. When considering nucleophilic sites (Figs. 3a to 3i), it can be observed that CO binds via its carbon atom to the metallic surfaces (Figs. 3a, 3b, 3d, 3e, 3 g and 3 h) while both C and O can be involved into the bonding to transition metal chalcogenide surfaces (Figs. 3c, 3f and 3i). On triangular nanostructures, CO is adsorbed via a bidendate mode and via mainly two metal–carbon bonds. On the MoO_2 triangular nanostructure, an additional Mo–O bond is formed. This yields a stronger adsorption energy (−2.971 eV) compared to Au and Cu nanostructures for which the adsorption energy read −2.002 and −2.345 eV, respectively. In the irregular hexagons and octagons (Figs. 3-b to 3-i), due to less charge transfer from the surface to the CO molecule, the monodentate adsorption mode prevails. This results in weaker adsorption energies (−0.492 to −1.59 eV).

As far as electrophilic sites are concerned, adsorption occurs via a weak interaction between the surface metallic atoms and the oxygen of the CO molecule (Figs. 4a and 4b). The weak charge transfer involved in the interaction yields very weak adsorption energies (0.03e for −0.071 eV and 0.012e for −0.027 eV, for the Au and Cu triangular nanostructures, respectively). Though the triangular MoO_2 and MoS_2 nanostructures show enhanced adsorption energies due to increased charge transfer from the molecule to the surface (Figs. 4c and 4d), the binding strength remains within the physisorption regime. However, irregular hexagonal and octagonal MoO_2 and MoS_2 nanostructures

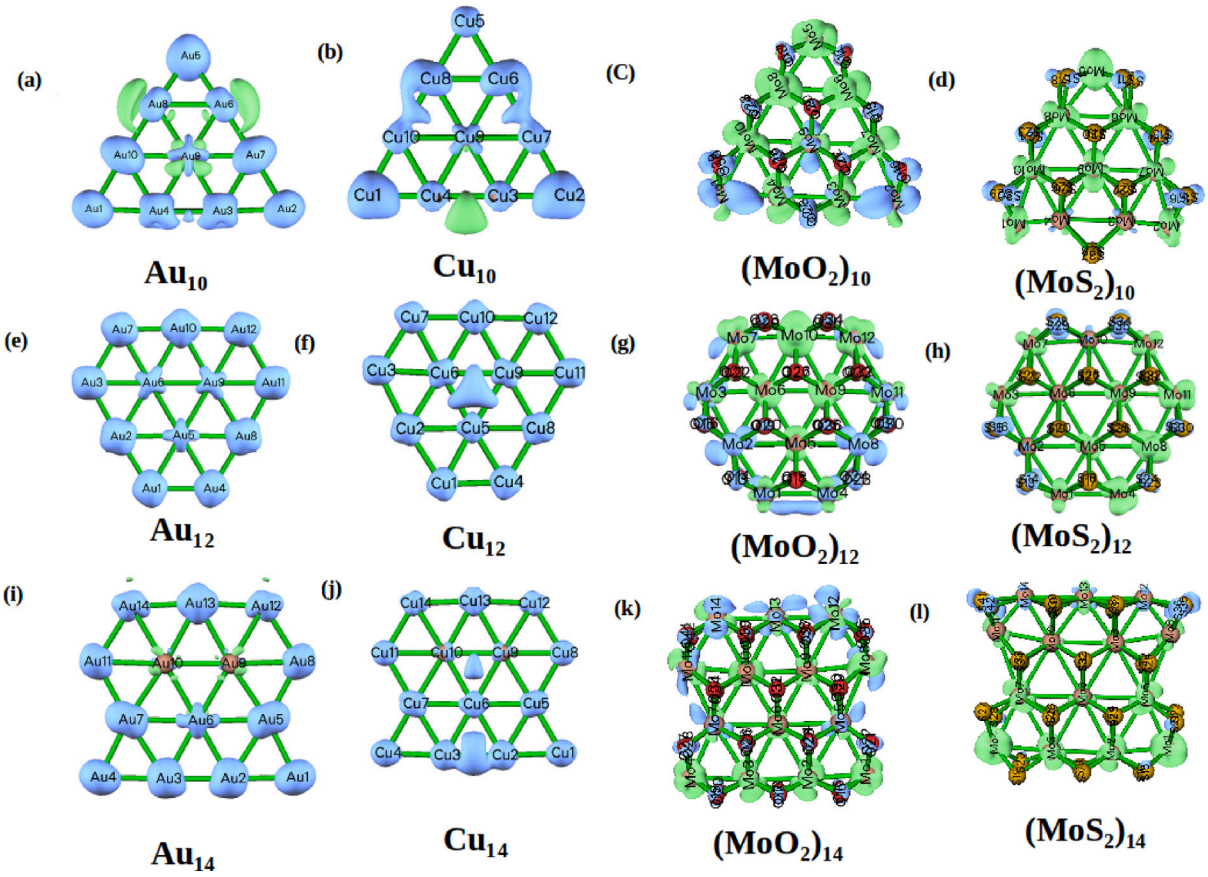

Fig. 2. Dual descriptor sites of the nanostructures, Orbital-weighted dual descriptor sites of the nanostructures, green/blue (Positive/negative values) represented susceptibility to electrophilic/nucleophilic attacks. The first, second and third rows: Au, MoO_2, Cu, MoS_2 clusters with x = 10, 12, 14 atoms and molecules. With atom colors: Au (brown), Cu (brown), Mo (brown), O (red) and S (gold).

show interesting features. A tridentate adsorption mode is observed on the irregular MoO_2 hexagon (Fig. 4e). The stabilization of three Mo to carbon (Mo-C) bonds leads to an adsorption energy of −2.462 eV. This adsorbate-surface interaction is weakened by about 600 meV on the hexagonal MoS_2 nanostructure (Fig. 4f). Only one Mo-C bond is formed. This may originate from steric effects induced by the larger sulfur atoms on the surface and that prohibit manifold bonding between the adsorbate and the surface atoms. The opposite trend is observed in octagonal nanostructures. A strong chemisorption is observed on MoS_2 (Fig. 4 h) while weaker bonding occurs on the MoO_2 nanostructure. This behavior may result from a subtle interplay between the nanostructure relaxation and the effective interaction energy between the CO molecule and the nanostructures. In fact compared to the surface free MoO_2 nanostructure displayed in (Fig. 1k), the surface in contact with CO undergoes considerable relaxation upon adsorption (Fig. 4 g).

To shed light on the nature of the interactions involved in the adsorption, we calculated the projected density of states (PDOS) of selected adsorption configurations reported in Figs. 3 and 4. The Figs. 5 and 6 show the PDOS for the nucleophilic and electrophilic sites, respectively. Because of their overall stronger adsorbate-surface interactions observed, the triangular and hexagonal nanostructures were considered in the former case, while irregular hexagonal and octagonal nanostructures were considered in the latter. In Fig. 5, we observe a weak hybridization in the energy range [−6, 0.5] eV, with the Fermi energy shifted to zero, between the 3d orbitals of Au (Cu) to which carbon monoxide binds and the 2p orbital of carbon. From 0.5 eV onwards, there is an hybridization in the conduction band, which reflects the electron-donating character of Au (Cu) nanoparticles. In contrast, for the MoO_2 and MoS_2 nanostructures, we observe strong hybridization between the 4d orbitals of Mo and the 2p orbital of carbon across the entire energy spectrum, indicating a strong bond between carbon monoxide and these nanoparticles. The same observations can be made in Fig. 6(a), (b), (c), and (d) for the MoO_2 and MoS_2 nanoparticles on electrophilic sites.

As already highlighted by the distribution of orbital-weighted dual descriptors (Fig. 2), the adsorption configurations of CO also support the greater reactivity of transition metal sites over chalcogens. The strong hybridization observed between the metal outermost d orbitals and carbon p orbitals support the prominent adsorption of CO by metal atoms and the strong adsorption energies reported in Figs. 3 and 4. O and Sulfur atoms are weakly reactive and would lead to negligible interaction energy with the CO molecule compared to transition metals. Thus the transition metal atoms play a more important role than the chalcogen atoms (O, S) in determining the adsorption energies and geometries of CO on the nanostructures. This corroborates well with a recent DFT study on the interplay between transition metals and chalcogens in the adsorption of NO and NO_2 on MoS_2, $MoSe_2$ and WS_2 TMDs [55]. The study showed that the binding via chalcogen atoms (S, Se) could only lead to very weak physisorption, independently on the nature of the transition metals (Mo, W).

4. Conclusion

We used DFT calculations to investigate the structure, stability and adsorption of CO on metallic and transition metal chalcogenide 2D nanostructures. Triangular, irregular hexagonal and octagonal 2D nanostructures with of 10, 12 and 14 Au, Cu, MoO_2 and MoS_2 motifs were found to be energically favorable and mechanically stable. We have determined the coordinative environment of the core and nanos-

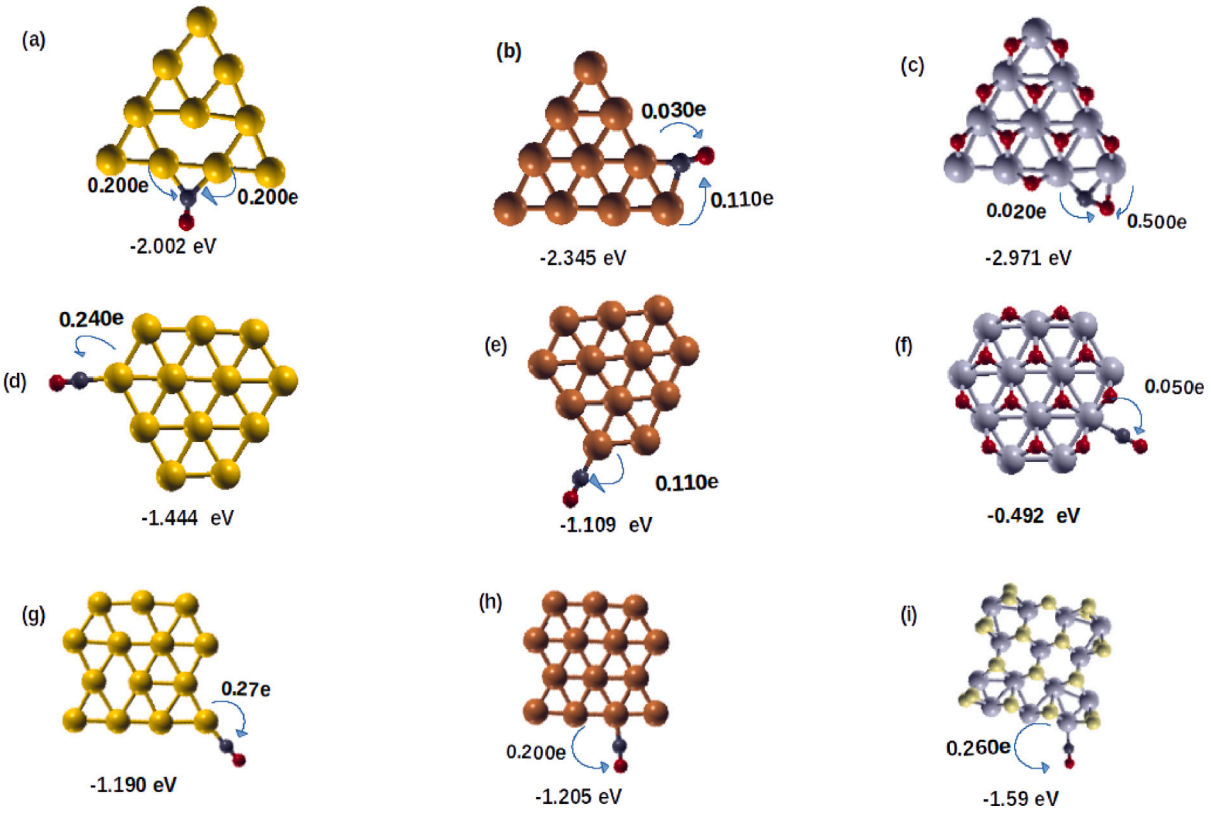

Fig. 3. Adsorption energies and Mulliken charge transfer differences on different nucleophilic attack sites of our CO/Au, CO/Cu, CO/MoO_2, CO/MoS_2 nanoparticles. With atom colors: Au (gold), Cu (brown), Mo (gray), O (red) and S (yellow), C (dark gray).

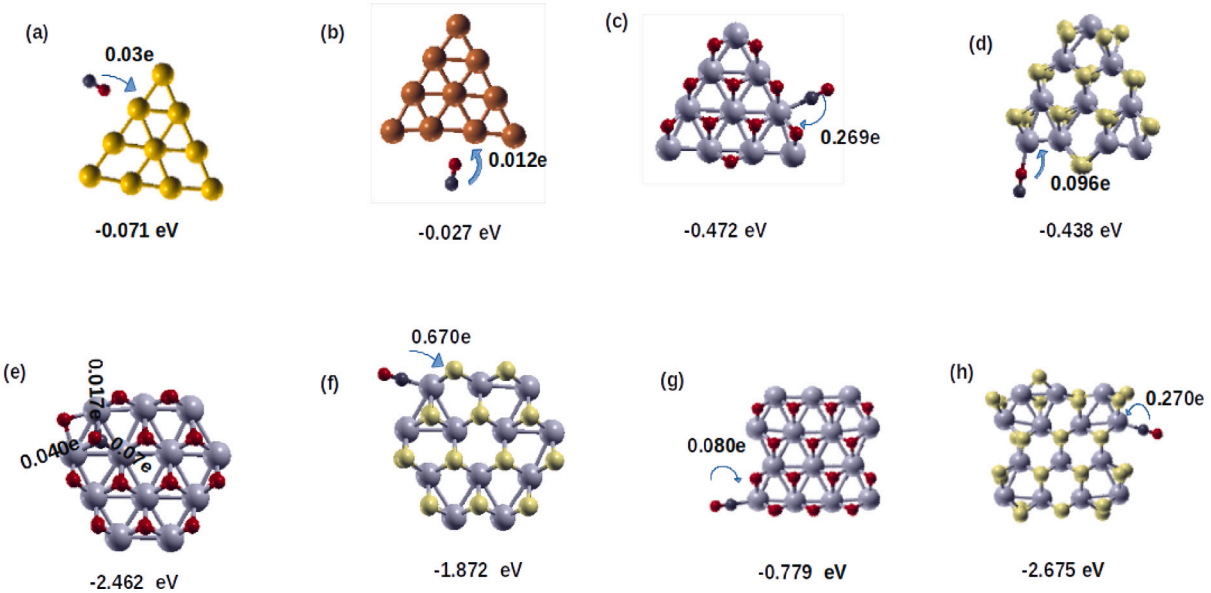

Fig. 4. Adsorption energies and Mulliken charge transfer differences on different Electrophile attack sites of our CO/Au, CO/Cu, CO/MoO_2, CO/MoS_2 nanoparticles. With atom colors: Au (gold), Cu (brown), Mo (gray), O (red) and S (yellow), C (dark gray).

tructures edges. The computed coordination numbers showed strongly undercordinated edge regions with higher charge density, trendsetting enhanced reactivity towards adsorption on these sites. The reactivity descriptors analysis highlighted a predominantly nucleophilic character of gold and copper-based nano-catalysts, while those based on MoO_2 and MoS_2 present both nucleophilic and electrophilic sites. The adsorption of carbon monoxide (CO) on the different nanostructures revealed that the interaction of CO with metallic nanoparticles is dominated by metal–carbon bonds on nucleophilic sites and by metal–oxygen bonds on electrophilic sites. Meanwhile, MoO_2 and MoS_2-based nanoparticles could establish strong bonds with CO both on electrophilic and nucleophilic sites.

The dispersion of gas molecule such as CO is a very huge concern as it is harmful for the ecosystem and the public health. Our work has explored the possibilities of sensors to toxic CO molecules based on low cost and abundant MoO_2 and MoS_2 materials and compared

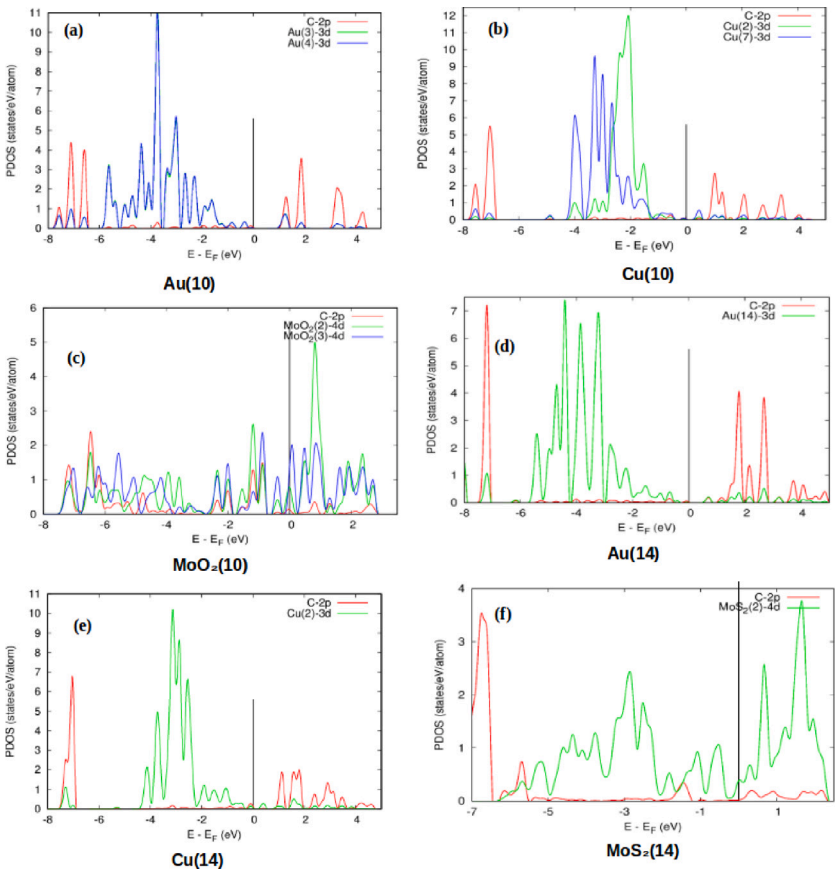

Fig. 5. The projected density (PDOS) of nucleophilic attack sites for our different nanostructures after CO adsorption. Figures (a), (b), (c), (d), (e), (f) correspond to the adsorption sites (a), (b), (c), (g), (h), (i) in Fig. 3.

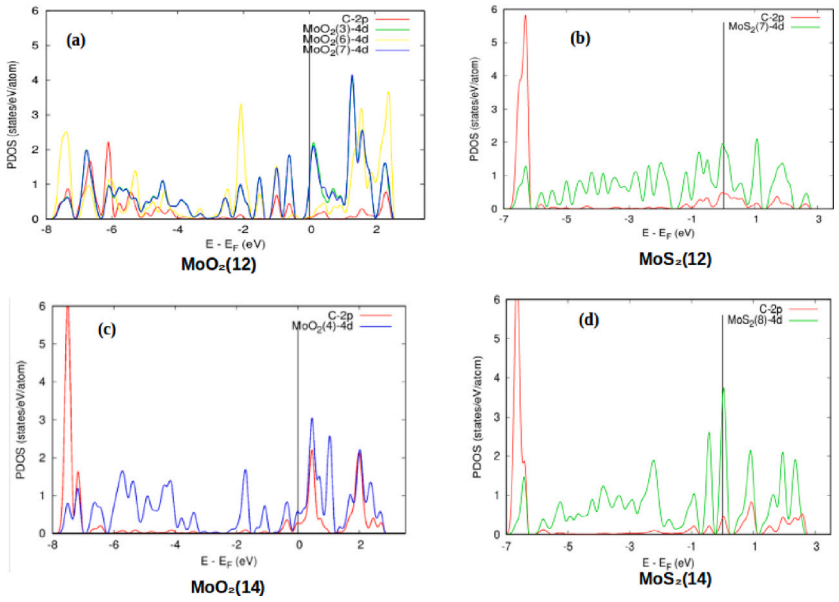

Fig. 6. The projected density (PDOS) of electrophilic attack sites for our different nanostructures after CO adsorption. Images (a), (b), (c), (d) correspond to adsorption sites (e), (f), (g), (h) in Fig. 4.

their behaviors with the expensive materials such as gold. By complementing existing knowledge about CO sensing by other abundant 2D materials [56,57], the present study contributes to lay the groundwork for understanding the basic sensing properties of 2D transition metal chalcogenides and the prerequisites for the further oxidation of CO.

CRediT authorship contribution statement

N. Ngom: Writing – review & editing, Writing – original draft, Visualization, Validation, Software, Project administration, Methodology, Investigation, Formal analysis, Data curation, Conceptualization.

A.J. Etindele: Writing – review & editing, Visualization, Validation, Supervision, Software, Project administration, Methodology, Investigation, Formal analysis, Data curation, Conceptualization. **N.F. Andriambelaza:** Writing – review & editing, Visualization, Resources. **C. Nithaya:** Validation, Supervision, Resources, Project administration, Methodology, Investigation, Conceptualization. **A.S. Wakata:** Validation, Supervision, Project administration, Methodology, Investigation, Conceptualization. **S. Kenmoe:** Writing – review & editing, Validation, Supervision, Project administration, Methodology, Investigation, Formal analysis, Conceptualization.

Declaration of competing interest

The authors declare that they have no known competing financial interests or personal relationships that could have appeared to influence the work reported in this paper.

Data availability

Data will be made available on request.

Acknowledgments

The authors acknowledge the Centre for High Performance Computing (CHPC), South Africa, for providing computational resources to this research project. We acknowledge support by the Open Access Publication Fund of the University of Duisburg-Essen.

Appendix A. Supplementary data

Supplementary material related to this article can be found online at https://doi.org/10.1016/j.comptc.2024.114877.

References

[1] Nidhi Gaur, Swati Sharma, Nitin Yadav, Environmental pollution, in: Green Chemistry Approaches to Environmental Sustainability, Elsevier, 2024, pp. 23–41.
[2] Aravindan Veiraiah, Carbon monoxide poisoning, Medicine 48 (3) (2020) 197–198.
[3] George W. Keulks, Charles C. Chang, Kinetics and mechanism of carbon monoxide oxidation over silver catalysts, J. Phys. Chem. 74 (13) (1970) 2590–2595.
[4] A.W. Smith, Oxidation of carbon monoxide on copper catalysts, J. Catalysis 4 (2) (1965) 172–183.
[5] Sébastien Royer, Daniel Duprez, Catalytic oxidation of carbon monoxide over transition metal oxides, ChemCatChem 3 (1) (2011) 24–65.
[6] Yang Lou, Jingyue Liu, CO oxidation on metal oxide supported single Pt atoms: the role of the support, Ind. Eng. Chem. Res. 56 (24) (2017) 6916–6925.
[7] Geoffrey C. Bond, David T. Thompson, Gold-catalysed oxidation of carbon monoxide, Gold Bull. 33 (2000) 41–50.
[8] Massimiliano Comotti, Wen-Cui Li, Bernd Spliethoff, Ferdi Schüth, Support effect in high activity gold catalysts for CO oxidation, J. Am. Chem. Soc. 128 (3) (2006) 917–924.
[9] Jin-Xun Liu, Ivo A.W. Filot, Yaqiong Su, Bart Zijlstra, Emiel J.M. Hensen, Optimum particle size for gold-catalyzed CO oxidation, J. Phys. Chem. C 122 (15) (2018) 8327–8340, PMID: 29707098.
[10] Yi Gao, Nan Shao, Yong Pei, Zhongfang Chen, Xiao Cheng Zeng, Catalytic activities of subnanometer gold clusters (Au16–Au18, Au20, and Au27–Au35) for CO oxidation, ACS Nano 5 (10) (2011) 7818–7829, PMID: 21888432.
[11] Eva M. Fernández, Pablo Ordejón, Luis C. Balbás, Theoretical study of O2 and CO adsorption on aun clusters (n=5–10), Chem. Phys. Lett. 408 (4) (2005) 252–257.
[12] Sahar Sharifzadeh, Patrick Huang, Emily Carter, Embedded configuration interaction description of CO on Cu(111): resolution of the site preference conundrum, J. Phys. Chem. C 112 (12) (2008) 4649–4657.
[13] Fang Xu, Kumudu Mudiyanselage, Ashleigh E. Baber, Markus Soldemo, Jonas Weissenrieder, Michael G. White, Dario J. Stacchiola, Redox-mediated reconstruction of copper during carbon monoxide oxidation, J. Phys. Chem. C 118 (29) (2014) 15902–15909.
[14] Sajedeh Manzeli, Dmitry Ovchinnikov, Diego Pasquier, Oleg V. Yazyev, Andras Kis, 2D transition metal dichalcogenides, Nat. Rev. Mater. 2 (8) (2017) 1–15.
[15] Fengwang Li, Mianqi Xue, Two-dimensional transition metal dichalcogenides for electrocatalytic energy conversion applications, Two-dimens. Mater.-Synth. Charact. Potential Appl. (2016) 64–84.
[16] Yandi Zhu, Ke Zhao, Jinlei Shi, Xiaoyan Ren, Xingju Zhao, Yuan Shang, Xinlian Xue, Haizhong Guo, Xiangmei Duan, Hao He, Zhengxiao Guo, Shunfang Li, Strain engineering of a defect-free, single-layer MoS2 substrate for highly efficient single-atom catalysis of CO oxidation, ACS Appl. Mater. Interfaces 11 (36) (2019) 32887–32894, PMID: 31429270.
[17] Agnieszka Kuc, Thomas Heine, Andras Kis, Electronic properties of transition-metal dichalcogenides, MRS Bull. 40 (7) (2015) 577–584.
[18] Mark T Greiner, Lily Chai, Michael G Helander, Wing-Man Tang, Zheng-Hong Lu, Transition metal oxide work functions: the influence of cation oxidation state and oxygen vacancies, Adv. Funct. Mater. 22 (21) (2012) 4557–4568.
[19] Qiang Fu, Jiecai Han, Xianjie Wang, Ping Xu, Tai Yao, Jun Zhong, Wenwu Zhong, Shengwei Liu, Tangling Gao, Zhihua Zhang, et al., 2D transition metal dichalcogenides: design, modulation, and challenges in electrocatalysis, Adv. Mater. 33 (6) (2021) 1907818.
[20] Liming Wang, Wenlong Chen, Doudou Zhang, Yaping Du, Rose Amal, Shizhang Qiao, Jianbo Wu, Zongyou Yin, Surface strategies for catalytic CO2 reduction: from two-dimensional materials to nanoclusters to single atoms, Chem. Soc. Rev. 48 (21) (2019) 5310–5349.
[21] Zahra Rafiei-Sarmazdeh, Seyed Morteza Zahedi-Dizaji, Aniseh Kafi Kang, Two-Dimensional Nanomaterials, IntechOpen London, UK, 2019.
[22] M. Goyal, M. Singh, Size and shape dependence of optical properties of nanostructures, Appl. Phys. A 126 (2020) 1–8.
[23] Hoa T. Phan, Amanda J. Haes, What does nanoparticle stability mean? J. Phys. Chem. C 123 (27) (2019) 16495–16507.
[24] Kevin Ndang Amassa, Anne Justine Etindele, Dick Hartmann Douma, Stephane Kenmoe, Chetty Nithaya, Ab initio study of p-and n-type doping of two-dimensional MoO2: investigation of a pn-homojunction, J. Phys. Commun. 8 (2) (2024) 025009.
[25] Riddhiman Medhi, Maria D. Marquez, T. Randall Lee, Visible-light-active doped metal oxide nanoparticles: review of their synthesis, properties, and applications, ACS Appl. Nano Mater. 3 (7) (2020) 6156–6185.
[26] Frank Abild-Pedersen, Martin P. Andersson, CO adsorption energies on metals with correction for high coordination adsorption sites–A density functional study, Surf. Sci. 601 (7) (2007) 1747–1753.
[27] Abhirup Patra, Haowei Peng, Jianwei Sun, John P. Perdew, Rethinking CO adsorption on transition-metal surfaces: Effect of density-driven self-interaction errors, Phys. Rev. B 100 (3) (2019) 035442.
[28] David Vázquez-Parga, Anabel Jurado, Alberto Roldan, Francesc Viñes, A computational map of the probe CO molecule adsorption and dissociation on transition metal low miller indices surfaces, Appl. Surf. Sci. 618 (2023) 156581.
[29] Charlie Tsai, Karen Chan, Jens K. Nørskov, Frank Abild-Pedersen, Understanding the reactivity of layered transition-metal sulfides: a single electronic descriptor for structure and adsorption, J. Phys. Chem. Lett. 5 (21) (2014) 3884–3889.
[30] Giannis Mpourmpakis, Antonis N. Andriotis, Dionisios G. Vlachos, Identification of descriptors for the CO interaction with metal nanoparticles, Nano Lett. 10 (3) (2010) 1041–1045.
[31] Yamei Zeng, Shiwei Lin, Ding Gu, Xiaogan Li, Two-dimensional nanomaterials for gas sensing applications: The role of theoretical calculations, Nanomaterials 8 (10) (2018).
[32] Xiao Tang, Aijun Du, Liangzhi Kou, Gas sensing and capturing based on two-dimensional layered materials: Overview from theoretical perspective, WIREs Comput. Mol. Sci. 8 (4) (2018) e1361.
[33] Paolo Giannozzi, Stefano Baroni, Nicola Bonini, Matteo Calandra, Roberto Car, Carlo Cavazzoni, Davide Ceresoli, Guido L. Chiarotti, Matteo Cococcioni, Ismaila Dabo, et al., QUANTUM ESPRESSO: a modular and open-source software project for quantum simulations of materials, J. Phys.: Condens. Matter 21 (39) (2009) 395502.
[34] M.J. Frisch, G.W. Trucks, H.B. Schlegel, G.E. Scuseria, M.A. Robb, J.R. Cheeseman, G. Scalmani, V. Barone, G.A. Petersson, H. Nakatsuji, et al., Gaussian 16 Revision C. 01. 2016, Gaussian Inc, Wallingford CT, 2016, 421.
[35] Debdutta Chakraborty, Pratim Kumar Chattaraj, Conceptual density functional theory based electronic structure principles, Chem. Sci. 12 (18) (2021) 6264–6279.
[36] Tian Lu, Feiwu Chen, Multiwfn: A multifunctional wavefunction analyzer, J. Comput. Chem. 33 (5) (2012) 580–592.
[37] Koichi Momma, Fujio Izumi, VESTA 3 for three-dimensional visualization of crystal, volumetric and morphology data, J. Appl. Crystallogr. 44 (6) (2011) 1272–1276.
[38] John P. Perdew, Kieron Burke, Matthias Ernzerhof, Generalized gradient approximation made simple, Phys. Rev. Lett. 77 (18) (1996) 3865.
[39] Stefan Grimme, Semiempirical GGA-type density functional constructed with a long-range dispersion correction, J. Comput. Chem. 27 (15) (2006) 1787–1799.
[40] Nicola Marzari, David Vanderbilt, Alessandro De Vita, M.C. Payne, Thermal contraction and disordering of the Al (110) surface, Phys. Rev. Lett. 82 (16) (1999) 3296.
[41] Carlo Adamo, Vincenzo Barone, Toward reliable density functional methods without adjustable parameters: The PBE0 model, J. Chem. Phys. 110 (13) (1999) 6158–6170.

[42] Yue Yang, Michael N. Weaver, Kenneth M. Merz Jr., Assessment of the "6-31+ G**+ LANL2DZ" mixed basis set coupled with density functional theory methods and the effective core potential: prediction of heats of formation and ionization potentials for first-row-transition-metal complexes, J. Phys. Chem. A 113 (36) (2009) 9843–9851.
[43] Qian Yang, Qiang Liang, Jun Liu, Shuquan Liang, Shasha Tang, Peijie Lu, Yakun Lu, Ultrafine MoO2 nanoparticles grown on graphene sheets as anode materials for lithium-ion batteries, Mater. Lett. 127 (2014) 32–35.
[44] Edney G.S. Firmiano, Marcos A.L. Cordeiro, Adriano C. Rabelo, Cleocir J. Dalmaschio, Antonio N. Pinheiro, Ernesto C. Pereira, Edson R. Leite, Graphene oxide as a highly selective substrate to synthesize a layered MoS2 hybrid electrocatalyst, Chem. Commun. 48 (2012) 7687–7689.
[45] K.T. Jacob, V.S. Saji, J. Gopalakrishnan, Y. Waseda, Thermodynamic evidence for phase transition in MoO2-δ, J. Chem. Thermodyn. 39 (12) (2007) 1539–1545.
[46] Masoud Shahrokhi, Pascal Raybaud, Tangui Le Bahers, On the understanding of the optoelectronic properties of S-doped MoO3 and O-doped MoS2 bulk systems: a DFT perspective, J. Mater. Chem. C 8 (2020) 9064–9074.
[47] Jeppe V. Lauritsen, Jakob Kibsgaard, Stig Helveg, Henrik Topsøe, Bjerne S. Clausen, Erik Lægsgaard, Flemming Besenbacher, Size-dependent structure of MoS2 nanocrystals, Nature Nanotechnol. 2 (1) (2007) 53–58.
[48] W. Liu, D. Liu, W.T. Zheng, Q. Jiang, Size and structural dependence of cohesive energy in Cu, J. Phys. Chem. C 112 (48) (2008) 18840–18845.
[49] Bun Chan, Wai-Leung Yim, Accurate computation of cohesive energies for small to medium-sized gold clusters, J. Chem. Theory Comput. 9 (4) (2013) 1964–1970, PMID: 26583547.
[50] Julien Engel, Samantha Francis, Alberto Roldan, The influence of support materials on the structural and electronic properties of gold nanoparticles – a DFT study, Phys. Chem. Chem. Phys. 21 (2019) 19011–19025.
[51] Deyao Wu, Cong Xi, Cunku Dong, Hui Liu, Xi-Wen Du, Bond-energy-integrated coordination number: An accurate descriptor for transition-metal catalysts, J. Phys. Chem. C 123 (46) (2019) 28248–28254.
[52] Ricardo Pino-Rios, Diego Inostroza, Gloria Cárdenas-Jirón, William Tiznado, Orbital-weighted dual descriptor for the study of local reactivity of systems with (quasi-) degenerate states, J. Phys. Chem. A 123 (49) (2019) 10556–10562.
[53] Hazem Abdelsalam, Qin Fang Zhang, Properties and applications of quantum dots derived from two-dimensional materials, Adv. Phys.: X 7 (1) (2022) 2048966.
[54] Hazem Abdelsalam, Mohamed H. Talaat, Igor Lukyanchuk, M.E. Portnoi, V.A. Saroka, Electro-absorption of silicene and bilayer graphene quantum dots, J. Appl. Phys. 120 (1) (2016) 014304.
[55] Piotr Radomski, Maciej J. Szary, Transition metals vs. chalcogens: The impact on NOx adsorption on MoS2, MoSe2 and WS2 transition-metal dichalcogenides, Acta Mater. 272 (2024) 119949.
[56] Omar H. Abd-Elkader, Mahmoud A.S. Sakr, Mohamed A. Saad, Hazem Abdelsalam, Qinfang Zhang, Electronic and gas sensing properties of ultrathin TiO2 quantum dots: A first-principles study, Results Phys. 52 (2023) 106804.
[57] H. Abdelsalam, N.H. Teleb, Baolin Wang, S. Yunoki, Qinfang Zhang, The electronic, adsorption, and catalytic properties of Bi-, Sb-, and As-nanoclusters, Catal. Today 376 (2021) 126–133, The 9th East Asia Joint Symposium on Environmental Catalysis and Eco-materials.